

VDE: Training-Free Accelerating Rectified Flow Model via Velocity Decomposition and Estimation

Junwen Tan Jinglin Liang Hongyuan Chen Shuangping Huang*
South China University of Technology

{eetjw, eelj1, 202230250013}@mail.scut.edu.cn, eehsp@scut.edu.cn



Figure 1. Qualitative comparison between VDE and standard 50-step sampling across Flux, Qwen-Image, and Wan2.1. VDE achieves almost the same visual quality with significantly reduced runtime.

Abstract

Though rectified flow models have achieved remarkable performance in image, video, and 3D generation, their practical deployments are challenged by slow inference speeds. Prior acceleration methods reuse cached features from previous steps, which neglects the growing mismatch between static caches and the evolving input, leading to reduced output fidelity. This work proposes Velocity Decomposition and Estimation (VDE), a training-free acceleration method that shifts the paradigm from caching-and-reusing to decomposing-and-estimating. Specifically, VDE decomposes the model’s velocity into components parallel and orthogonal to the input, exploiting their temporal predictability and directional stability for precise, input-adaptive estimation. To prevent error accumulation, it periodically anchors the model’s state via full forward passes. Extensive experiments on image and video generation tasks demonstrate that VDE achieves substantial acceleration with minimal loss in visual quality. Notably, VDE accelerates Flux by $3.22\times$ and achieves an LPIPS of 0.069 on Qwen-Image, outperforming the best baseline with a 52.2% reduction. Code: <https://github.com/Tan-Junwen/VDE>

1. Introduction

Recently, rectified flow models have achieved strong performance in image[1, 8, 48], video[14, 16, 46], and 3D asset synthesis[13, 18, 19, 22, 49]. However, their inference typically requires executing dozens of iterative sampling steps, leading to high latency and limited deployment in real-time or compute-constrained scenarios.

To mitigate the high inference cost, training-free acceleration methods [6, 17, 27, 30, 53] have gained significant traction. These approaches typically follow a *cache-and-reuse* paradigm, where intermediate features from previous steps are stored and reused in subsequent steps to skip redundant computation. For example, some methods [7, 15, 53] cache and reuse the outputs of attention layers, while other methods like TeaCache [26] and Easy-Cache [56] cache and reuse the residuals of Transformer blocks and the residuals of the whole model, respectively. Although these methods may trigger reusing based on a low rate-of-change in certain metrics, the fundamental mismatch between the static cache and the dynamic input inevitably propagates into the model’s output. This cache-input mismatch results in an output-input mismatch, where the approximated output fails to accurately respond to the current input state, ultimately degrading the visual fidelity of generated content.

* Corresponding author.

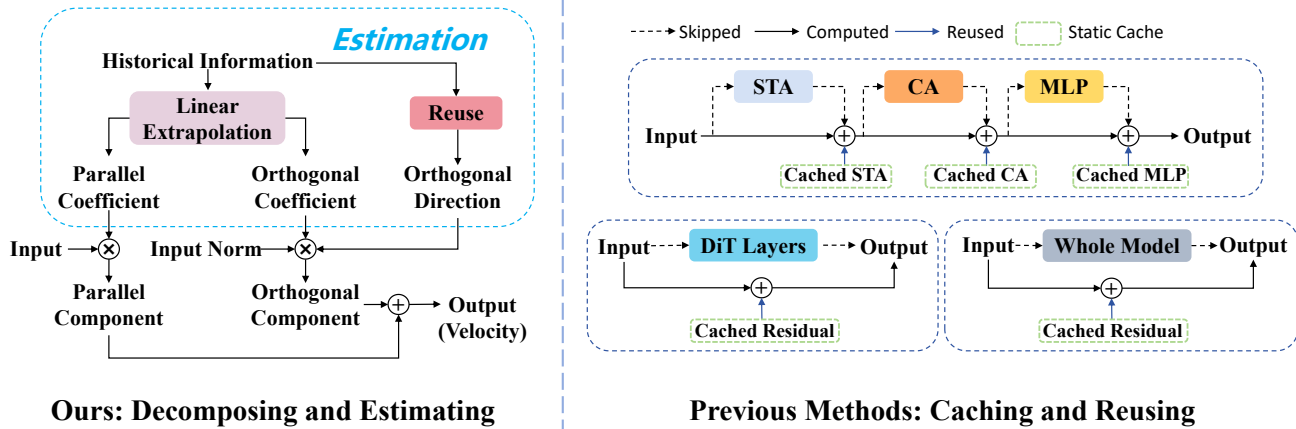


Figure 2. Comparison between standard feature caching and our VDE. **Left:** VDE decomposes the velocity into parallel and orthogonal components, estimating their evolution via linear extrapolation and directional reuse to ensure adaptive, input-aligned estimation. **Right:** Prior methods reuse static features, which fail to evolve with the dynamic input and inherently cause cache-input mismatch.

In this work, we revisit training-free acceleration and propose **Velocity Decomposition and Estimation (VDE)**, a novel method that replaces the static cache reusing with estimation of output directly from the current input via an estimation function, thereby fundamentally eliminating the output-input mismatch caused by cache-input mismatch. This estimation is built upon the discovery of a robust regularity in the model’s input-output behavior during sampling. Specifically, we observed that after decomposing the velocity of models into components parallel and orthogonal to the input, there is a stable phase where two consistent patterns appear. First, the scalar coefficients of components evolve smoothly over time, showing strong local linearity between consecutive steps. This property enables reliable estimation of them based on their recent historical values. Second, the orthogonal direction remains largely constant over short intervals, allowing it to be safely reused for multiple adjacent steps without significant error. Based on these insights, VDE constructs an estimation function that dynamically computes the velocity from the current input. Concretely, VDE first executes model inference at periodic anchor steps and decomposes model-predicted velocity to obtain the scalar coefficients and orthogonal direction. Then VDE estimates the coefficients of subsequent steps by linear extrapolation based on their historical values from recent steps and reuse the latest orthogonal direction. The estimated velocity is then synthesized by combining the current input with the extrapolated coefficients and the orthogonal direction. Crucially, unlike caching-based strategies, VDE is inherently input-adaptive—each estimated output is freshly constructed from the current input, eliminating the use of stale features and enabling high-fidelity generation alongside substantial speedups.

Our main contributions are summarized as follows:

- We identify the **cache-input mismatch** problem in existing caching-based acceleration methods and review training-free acceleration as estimating the model’s input-output mapping.
- We propose **VDE**, a novel method that shifts the acceleration paradigm from caching-and-reusing to decomposing-and-estimating, enabling precise, input-adaptive estimation of model outputs.
- Extensive experiments on image and video generation demonstrate that VDE achieves $2.04\text{-}3.22\times$ speedups with superior visual fidelity, reducing LPIPS by 52.2% on Qwen-Image against the best baseline.

2. Related Work

2.1. Rectified Flow Model

Diffusion models have dominated high-quality visual generation [11, 32, 36, 37, 43]. Recent transformer-based architectures such as DiT [33] and related scalable variants [4, 5, 23] further push generation fidelity. Rectified Flow (RF) models [8, 25] reformulate generation as integrating an ODE-driven velocity field, enabling stable training and state-of-the-art synthesis across image [1, 3, 8, 48], video [14, 16, 46, 55], and 3D [13, 18, 19, 22, 49, 51] modalities. Despite their versatility, the sequential nature of RF inference remains computationally demanding, motivating the pursuit of efficient acceleration methods.

2.2. Training-Free Acceleration Methods.

Existing acceleration techniques can be broadly grouped into two categories: (1) training-based methods such as distillation [28, 31, 38, 39], quantization [10, 21, 41, 42], consistency training [29, 44, 45, 47] and architecture compression/search [20, 20, 54], and (2) training-free methods

[6, 17, 27, 30]. Since training-based methods require additional data and optimization cycles and often reduce generalization ability, training-free methods have emerged as a promising alternative. Early caching methods for U-Net [2, 35, 37] architectures, such as DeepCache[30] and Faster Diffusion[17], exploit spatial redundancy by reusing high-level feature maps across nearby timesteps. FORA [40], Δ -DiT [6] and T-GATE [27] extended this idea to DiT architectures, achieving inference speedup in image generation. For video generation, PAB [53] broadcasts attention outputs in a variance-aware pyramid schedule to maximize reuse. AdaCache [15] adjusts feature caching strategies based on content complexity. TeaCache [26] introduces a timestep-embedding-aware indicator and a rescaling strategy to better predict reuse reliability. EasyCache [56] moves toward runtime adaptivity, dynamically reusing previously computed features without offline profiling. OmniCache [7] investigates the generation trajectories across samples and uses curvature-guided selection to skip redundant steps. While effective, these methods reuse stale features, inevitably causing cache-input mismatches that accumulate errors and degrade fidelity.

3. Methodology

3.1. Problem Formulation

This work focuses on accelerating Rectified Flow (RF) models [8, 25], which learn a continuous-time generative process to transport data from a noise distribution p_0 to a data distribution p_1 . Given a data sample x_1 and Gaussian noise $x_0 \sim \mathcal{N}(0, I)$, an intermediate latent at time $t \in [0, 1]$ is constructed via linear interpolation:

$$x_t = tx_1 + (1 - t)x_0. \quad (1)$$

The core of RF model is to predict a velocity, defined as the time derivative of this path:

$$\mathbf{v}_t = \frac{dx_t}{dt} = x_1 - x_0. \quad (2)$$

During inference, the model u_θ predicts an instantaneous velocity $v_t = u_\theta(x_t, c, t)$ at each step, which guides the sample x_t from the initial noise x_0 towards the final data sample x_1 via numerical integration of the ODE $\frac{dx_t}{dt} = v_t$.

We formulate the problem of training-free acceleration for such models as the task of constructing a lightweight estimation function f_{est} . The goal of this function is to accurately approximate the model’s velocity output without performing a full forward pass, thereby reducing computational cost. Formally, we aim to obtain:

$$\hat{v}_t = f_{\text{est}}(x_t, t, I_{\text{hist}}), \quad (3)$$

where \hat{v}_t is the estimated velocity, x_t is the current latent input, t is the timestep, and I_{hist} encapsulates any lightweight

historical information from previous steps (e.g., past latents, velocities, or cached features). A well-designed f_{est} allows us to skip the majority of the model’s forward passes while maintaining the visual fidelity of the generated content.

3.2. Temporal Dynamics of Velocity Components

To analyze the temporal behavior of the model, we first introduce an exact decomposition of the velocity output v_t with respect to the input x_t . This decomposition forms the basis for our empirical analysis.

Velocity Decomposition. The velocity v_t at any timestep can be uniquely decomposed into a component parallel to the latent x_t and an orthogonal component:

$$v_t = \alpha_t x_t + \beta_t \|x_t\| u_t, \quad (4)$$

where $\alpha_t, \beta_t \in \mathbb{R}$ are scalar coefficients and $u_t \in \mathbb{R}^d$ is a unit vector satisfying $u_t^\top x_t = 0$.

Given v_t from a model forward pass, the decomposition is computed as follows. The coefficient of the parallel component is:

$$\alpha_t = \frac{\langle v_t, x_t \rangle}{\|x_t\|^2}. \quad (5)$$

The orthogonal residual is then:

$$r_t = v_t - \alpha_t x_t. \quad (6)$$

Finally, the unit orthogonal direction and its normalized coefficient are obtained by:

$$u_t = \frac{r_t}{\|r_t\|}, \quad \beta_t = \frac{\|r_t\|}{\|x_t\|}. \quad (7)$$

Thus, the tuple (α_t, β_t, u_t) provides a complete parameterization of v_t relative to x_t .

Empirical Findings. Although the decomposition in Eq. 4 provides an analytical form for the velocity, the tuple (α_t, β_t, u_t) remains unknown before executing the model at timestep t . To understand the behavior of these variables, we analyze 500 samples for each model and apply the decomposition across all timesteps for each sample. Our analysis reveals strong and consistent temporal regularities. As shown in Fig. 3, after an initial *warm-up phase*, the sampling trajectory enters a *stable phase* characterized by two patterns: (1) **Predictable Coefficients.** The scalar coefficients α_t and β_t evolve smoothly and demonstrate strong local linearity between consecutive steps. This regularity enables their reliable estimation via extrapolation from recent historical values. (2) **Stable Orthogonal Direction.** The unit direction u_t remains nearly constant over short intervals, with cosine similarity between adjacent steps typically exceeding 0.99. This permits its safe reuse across multiple steps without introducing significant error.

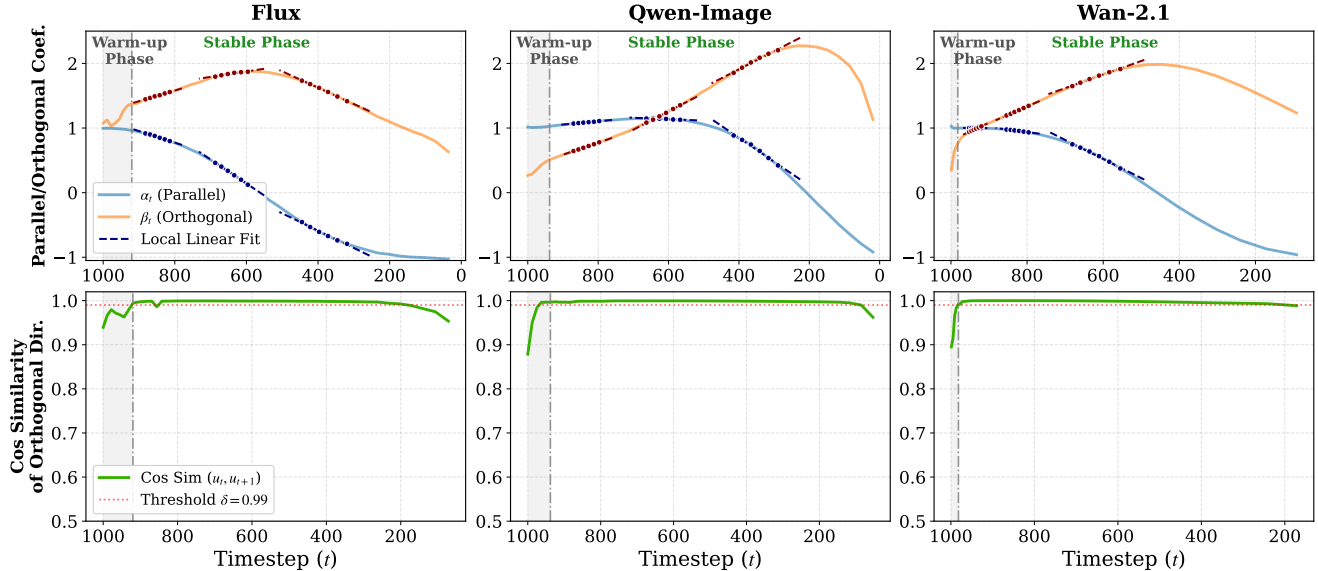


Figure 3. **Temporal dynamics of velocity components.** Evolution of the decomposed velocity components across Flux, Qwen-Image, and Wan2.1. **Top:** The parallel (α_t) and orthogonal (β_t) coefficients. **Bottom:** The cosine similarity of adjacent orthogonal directions (u_t). After an initial warm-up phase (shaded), the scalar coefficients evolve smoothly with strong local linearity, while the orthogonal direction remains highly stable (cosine similarity ≈ 1). These regularities enable VDE’s coefficient estimation and direction reuse.

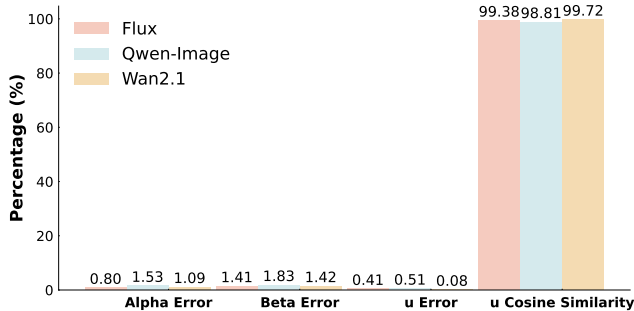


Figure 4. Quantitative evidence for the temporal regularities. We report prediction errors of decomposed velocity components under a two-step linear extrapolation. Both scalar coefficients show extremely low errors, while the orthogonal direction maintains high cosine similarity, confirming their local linearity and short-term stability, respectively.

The quantitative results in Fig. 4 robustly support these observations. When employing linear extrapolation during stable phase over an interval of two steps, the coefficients demonstrate remarkably low prediction errors (α error: 0.80%, 1.53%, 1.09%; β error: 1.41%, 1.83%, 1.42% across models), confirming the local linearity. Similarly, reusing the orthogonal direction introduces minimal error (0.41%, 0.51%, 0.08%), unequivocally validating its stability. Collectively, these findings imply that, during the stable phase, the velocity v_t can be accurately estimated by analytically propagating its decomposed components, bypassing the need for a full model forward pass at every step.

Definition and Identification of the Stable Phase. For-

mally, we define that the denoising process enters the stable phase at step i if and only if the linear extrapolation from steps i and $i + 1$ accurately predicts step $i + 2$, and the orthogonal direction remains stable. This is satisfied when the following criteria are met:

$$\begin{cases} \max \left(\frac{|\hat{\alpha}_{i+2} - \alpha_{i+2}|}{|\alpha_{i+2}|}, \frac{|\hat{\beta}_{i+2} - \beta_{i+2}|}{|\beta_{i+2}|} \right) < \epsilon \\ u_i^\top u_{i+1} > \delta \end{cases}, \quad (8)$$

where $\hat{\alpha}_{i+2}$ and $\hat{\beta}_{i+2}$ are the linearly extrapolated coefficients based on steps i and $i + 1$. We empirically set the thresholds to $\epsilon = 0.02$ and $\delta = 0.99$. While this formal formulation enables practical dynamic detection, our extensive profiling across 10,000 trajectories confirms that this transition consistently occurs in the first few steps. To ensure the model reliably establishes the global outline during early denoising steps, we set a conservatively fixed warm-up step in our main experiments. Detailed statistical analysis is provided in the supplementary material.

3.3. Our VDE Method

Building on the above observations, we detail the Velocity Decomposition and Estimation (VDE) method. VDE leverages the predictability of the coefficients and the stability of the orthogonal direction to construct an estimation function. The runtime procedure of VDE is as follows. In the initial *warm-up phase*, we perform a full model inference at every step. Upon entering the *stable phase*, VDE switches to



Figure 5. Qualitative comparison of caching-based methods and our VDE on Flux. VDE preserves both global structure and fine details.

an anchor-and-estimate mode. At periodic anchor steps, a full model inference is executed, and the velocity is decomposed to obtain the ground-truth tuple (α_t, β_t, u_t) . For all subsequent non-anchor steps until the next anchor, the velocity is estimated without model computation. The estimation for a non-anchor step t is performed by first predicting the scalar coefficients via linear extrapolation from the two most recent anchors at $t_1 > t_2$:

$$\hat{\alpha}_t = \alpha_{t_1} + \frac{\alpha_{t_2} - \alpha_{t_1}}{t_2 - t_1}(t - t_1), \quad \hat{\beta}_t = \beta_{t_1} + \frac{\beta_{t_2} - \beta_{t_1}}{t_2 - t_1}(t - t_1). \quad (9)$$

The orthogonal unit direction is reused from the most recent anchor:

$$\hat{u}_t = u_{t_2}. \quad (10)$$

The final velocity estimate is then synthesized analytically by combining these components with the current input x_t :

$$\hat{v}_t = f_{\text{est}}^{\text{VDE}}(x_t, t, I_{\text{hist}}) = \hat{\alpha}_t x_t + \hat{\beta}_t \|x_t\| \hat{u}_t. \quad (11)$$

Explicitly depending on x_t , this estimation is inherently input-adaptive and leverages observed temporal regularities. Decomposition and estimation involves only straightforward arithmetic operations between variables, at a negligible computational cost compared to a full model evaluation.

The anchor interval controls the speed-quality trade-off: a larger interval yields higher acceleration but may slightly degrade visual fidelity. Empirically, a two-step interval during the stable phase provides an optimal balance.

4. Experiment

4.1. Settings

Base Models and Compared Methods. We evaluate the performance of our method on various models, including FLUX.1 [dev] [1] and Qwen-Image [48] for image generation, and Wan2.1-1.3B [46] for video generation. All experiments are conducted on NVIDIA A800 80GB GPUs with Pytorch. We compare VDE with representative training-free acceleration baselines, including Δ -DiT[6], T-GATE [27], PAB [53], TeaCache [26], and EasyCache [56], and report results of naively reducing steps.

Evaluation Metrics. To assess the effectiveness of our method, we consider both efficiency and visual quality. The efficiency is measured by latency, speedup, and Number of Function Evaluations (NFE). For image generation tasks, we use SSIM, PSNR, and LPIPS [9, 52] to assess visual retention, human-aligned metrics (e.g., ImageReward [50])

Flux			Qwen-Image			Wan2.1		
T=50	TeaCache	VDE(Ours)	T=50	TeaCache	VDE(Ours)	T=50	TeaCache	VDE(Ours)
8.20s	3.12s (2.63×)	3.04s (2.70×)	12.53s	4.66s (2.69×)	4.64s (2.70×)	175.35s	87.77s (2.00×)	70.11s (2.50×)
8.20s	2.81s (2.91×)	3.04s (2.70×)	12.53s	4.62s (2.71×)	4.64s (2.70×)	175.35s	69.11s (2.54×)	70.11s (2.50×)
T=50	EasyCache	VDE(Ours)	T=50	EasyCache	VDE(Ours)	T=50	EasyCache	VDE(Ours)

Figure 6. Qualitative comparison of caching-based methods and our VDE on Flux, Qwen-Image, and Wan2.1. VDE successfully accelerates generation while maintaining visual fidelity comparable to the $T=50$ baseline. In contrast, caching-based methods often exhibit texture degradation or structural inconsistencies due to cache-input mismatch.

to validate perceptual fidelity, and CLIP [34] for semantic alignment. For video generation tasks, we apply SSIM, PSNR, and LPIPS to assess visual retention, and evaluate performance using the VBench [12] framework.

Implementation Details. All experiments are carried out on NVIDIA A800 80GB GPUs with PyTorch. For FLUX.1 [dev], we evaluate three VDE variants: each runs the first 7 steps and the final step, and uses intervals of 2, 3, or 4 steps in between. For Qwen-Image, we evaluate two VDE variants: each runs the first 11 steps and the final step, and uses intervals of 2 or 5 steps in between. For Wan2.1, we evaluate two VDE variants: one runs the first 11 steps and the final step with a 2-step interval, and the other runs the first 9 steps and the final step with a 4-step interval. For image generation tasks, we randomly select 1000 samples from the MS-COCO 2017 [24] validation set, using a resolution of 512×512 for all images. For video generation, we test our approach based on the VBench framework [12], generating 5 videos for each of 946 benchmark prompts. These videos are comprehensively evaluated across 16 aspects proposed in the VBench evaluation system.

4.2. Main Results

Quantitative Results on Image Generation. Tab. 1 reports the efficiency–fidelity trade-off on FLUX.1 [dev] and Qwen-Image. For reference, we include: (1) the original sampler with $T=50$ steps, (2) reduced-step baselines with comparable speedups, and (3) fast/slow variants of TeaCache and EasyCache that respectively favor speed or quality. We additionally evaluate three variants of VDE (fast/medium/slow) to cover different latency budgets. Across both base models, VDE consistently achieves a superior speed–quality balance. On FLUX.1 [dev], **VDE-fast** matches the latency of EasyCache-fast ($3.01 \times$ vs. $2.91 \times$ speedup) by effectively reducing the NFE to 16, yet it delivers substantially higher visual retention, improving SSIM from 0.7240 to 0.8267 and LPIPS from 0.3197 to 0.1997. **VDE-medium** further improves reconstruction fidelity with just 18 NFEs while maintaining a competitive $2.70 \times$ speedup. **VDE-slow** achieves the highest visual retention overall. It obtains a $2.21 \times$ speedup while preserving nearly identical visual quality, outperforming the best baseline EasyCache-slow by 19.5% in SSIM, 30.3% in PSNR,

Table 1. Quantitative comparison in image generation on FLUX.1 [dev] and Qwen-Image. Baseline sampling uses $T=50$ steps.

Methods	Efficiency			Visual Retention			CLIP \uparrow	ImageReward \uparrow
	Speedup \uparrow	Latency (s) \downarrow	NFE \downarrow	SSIM \uparrow	PSNR \uparrow	LPIPS \downarrow		
FLUX.1 [dev] [1] (512\times512)								
$T = 50$	1.00 \times	8.20	50	-	-	-	0.3090	0.976
$T = 24$	2.06 \times	3.98	24	0.7512	19.74	0.2264	0.3092	0.989
$T = 18$	2.71 \times	3.03	18	0.6862	17.79	0.3367	0.3104	0.991
Teacache-fast [26]	2.63 \times	3.12	-	0.6858	18.07	0.3355	0.3099	0.988
Teacache-slow [26]	1.87 \times	4.39	-	0.7241	19.12	0.2941	0.3089	0.990
Easycache-fast [56]	2.91 \times	2.81	-	0.7240	19.59	0.3197	0.3109	0.986
Easycache-slow [56]	2.09 \times	3.92	-	0.7428	19.81	0.2793	0.3096	0.980
VDE-fast (Ours)	3.01 \times	2.72	16	0.8267	23.19	0.1997	0.3109	0.969
VDE-medium (Ours)	2.70 \times	3.04	18	0.8499	24.02	0.1679	0.3102	0.973
VDE-slow (Ours)	2.21 \times	3.70	22	0.8877	25.81	0.1243	0.3095	0.978
Qwen-Image [48] (512\times512)								
$T = 50$	1.00 \times	12.53	100	-	-	-	0.3156	1.295
$T = 24$	2.06 \times	6.09	48	0.8293	22.31	0.1744	0.3158	1.281
$T = 18$	2.71 \times	4.62	36	0.7654	19.84	0.2403	0.3164	1.286
Teacache-fast [26]	2.69 \times	4.66	-	0.5596	14.43	0.4773	0.3116	0.948
Teacache-slow [26]	1.75 \times	7.17	-	0.5573	13.99	0.4495	0.3118	1.121
Easycache-fast [56]	2.71 \times	4.62	-	0.7027	19.84	0.4239	0.3209	0.992
Easycache-slow [56]	1.97 \times	6.36	-	0.8708	23.83	0.1445	0.3153	1.282
VDE-fast (Ours)	2.70 \times	4.64	36	0.8967	25.46	0.1096	0.3163	1.287
VDE-slow (Ours)	2.04 \times	6.14	48	0.9362	28.58	0.0691	0.3159	1.295

Table 2. Quantitative comparison in video generation on Wan-2.1. Baseline sampling uses $T=50$ steps.

Methods	Efficiency			Visual Retention			VBench (%) \uparrow
	Speedup \uparrow	Latency (s) \downarrow	NFE \downarrow	SSIM \uparrow	PSNR \uparrow	LPIPS \downarrow	
Wan2.1-1.3B [46] (81 frames, 832\times480)							
$T = 50$	1 \times	175.35	100	-	-	-	81.30
$T = 24$	2.08 \times	84.17	48	0.5939	15.47	0.3690	80.73
$T = 20$	2.50 \times	70.10	40	0.5226	14.50	0.4374	80.30
Random 0.4	2.45 \times	71.69	-	0.4204	11.92	0.5911	78.68
Static cache	2.45 \times	71.54	-	0.5007	14.18	0.4789	79.58
PAB [53]	1.72 \times	102.03	-	0.6484	18.84	0.3010	77.60
TeaCache [26]	2.00 \times	87.77	-	0.8057	22.57	0.1277	81.04
EasyCache [56]	2.54 \times	69.11	-	0.8337	25.24	0.0952	80.49
VDE-fast (ours)	2.50 \times	70.11	40	0.8658	24.69	0.0754	80.43
VDE-slow (ours)	2.08 \times	84.18	48	0.8902	25.92	0.0554	80.32

and reducing LPIPS by 55.4%. Furthermore, VDE exhibits excellent perceptual fidelity on human-aligned evaluations. Notably, VDE-slow achieves an ImageReward of 1.295 on Qwen-Image, which matches the full $T=50$ baseline. This demonstrates that our estimation yields output quality nearly indistinguishable from the original $T=50$ baseline while drastically reducing computation.

Quantitative Results on Video Generation. We further evaluate VDE on video generation with Wan2.1. As summarized in Table 2, VDE achieves competitive speedup (reducing NFEs from 50 to 20-24) while attaining the best visual retention. It outperforms other approaches in both structural and perceptual similarity metrics, and maintains a VBench score close to the original model. These results

Table 3. Ablation on substituting true vs. estimated decomposition components on FLUX.1 [dev], 512×512 resolution. The estimated values are obtained on the setting of inference in the first 9 steps and the last step, with an interval of 2 steps in between.

Setting	SSIM ↑	PSNR ↑	LPIPS ↓	CLIP ↑
True u_t	0.9893	40.79	0.0132	0.3089
True β_t	0.9262	28.76	0.0874	0.3097
True α_t	0.9263	28.78	0.0860	0.3097
True u_t, β_t	0.9916	41.79	0.0100	0.3089
True u_t, α_t	0.9899	41.02	0.0124	0.3089
True α_t, β_t	0.9265	28.78	0.0874	0.3098
Estim. α_t, β_t, u_t	0.8931	26.15	0.1198	0.3095

Table 4. Comparison of different anchor intervals on FLUX.1 [dev]. The inference is fixed in the first 7 steps and the last step, with an interval of n steps in between. The resolution is 512×512.

Interval	Efficiency	Visual Retention			CLIP ↑
	Speedup ↑	SSIM ↑	PSNR ↑	LPIPS ↓	
$n = 1$	1.69×	0.9283	28.76	0.0801	0.3093
$n = 2$	2.21×	0.8877	25.81	0.1243	0.3095
$n = 3$	2.70×	0.8499	24.02	0.1679	0.3102
$n = 4$	3.01×	0.8267	23.19	0.1997	0.3109
$n = 5$	3.22×	0.8064	22.56	0.2168	0.3110

Table 5. Comparison of different resolutions and aspect ratio on Qwen-Image. The inference is fixed in the first 11 steps and the last step, with an interval of 2 steps in between.

Resolution	Efficiency	Visual Retention			CLIP ↑
	Speedup ↑	SSIM ↑	PSNR ↑	LPIPS ↓	
256×256	2.07×	0.9079	26.93	0.1036	0.3149
512×512	2.04×	0.9354	28.50	0.0697	0.3159
1024×768	2.05×	0.9584	30.40	0.0564	0.3150
1024×1024	2.06×	0.9482	30.59	0.0541	0.3170

confirm VDE as an effective training-free accelerator that delivers a superior speed–fidelity trade-off.

Visualization. Fig. 5 and Fig. 6 qualitatively compare VDE against training-free baselines (EasyCache, TeaCache) and the original $T=50$ model. While EasyCache and TeaCache effectively reduce steps, their outputs deviate noticeably from the $T=50$ baseline, exhibiting softened textures, weakened high-frequency details, and compromised fine structures. In contrast, VDE closely matches the $T=50$ baseline, preserving global composition and local details (e.g., shapes, textures, shading). This demonstrates that VDE better maintains the generative trajectory and mitigates cache-input mismatches, yielding highly faithful outputs alongside substantial acceleration.

4.3. Ablation Studies

Effect of Decomposition Components. We first examine how each component in the velocity decomposition affects reconstruction quality. Tab. 3 reports results when substituting the true orthogonal direction u_t or the scalar coefficients (α_t, β_t) with their estimated counterparts. Replacing the true coefficients with our estimates yields nearly lossless reconstruction (e.g., SSIM 0.9893), confirming that the coefficient estimation is highly accurate. Replacing the true u_t with the cached direction introduces a moderate quality drop but remains stable, indicating that reusing the orthogonal unit direction is a controlled and low-error approximation. When all components are estimated jointly, VDE maintains reasonable reconstruction fidelity, validating that the velocity decomposition can be reliably inferred online without requiring ground-truth intermediate states.

Anchor Interval. We further study the effect of the inference interval n , which determines how frequently the velocity decomposition is updated during sampling. The anchor interval controls the trade-off between speed and quality. A larger interval yields higher acceleration but may slightly degrade visual fidelity. Tab. 4 shows that reducing the update frequency (larger n) improves efficiency but gradually decreases visual retention. Notably, $n=2$ achieves the best speed–quality balance, providing a 2.21× speedup while retaining high fidelity, which corresponds to the VDE-slow configuration reported in the main results.

Resolution and Aspect Ratio Generalization. Finally, we evaluate VDE under varying output resolutions and aspect ratios on Qwen-Image (Tab. 5). Across 256×256 to 1024×1024, VDE maintains consistent speedups (2×) and stable visual retention, indicating that our method scales robustly with spatial resolution. Importantly, CLIP scores remain nearly unchanged, demonstrating that the semantic alignment is preserved even when image complexity increases. These results verify that VDE is resolution-agnostic and generalizes well across modern diffusion model deployment settings.

5. Conclusion

We presented Velocity Decomposition and Estimation (VDE), a training-free acceleration framework for rectified flow models. This work provides a new perspective by formulating acceleration as estimating the model’s output from the current input. Instead of caching and reusing static features, VDE decomposes the velocity into parallel and orthogonal components and performs lightweight online estimation. This shifts the acceleration paradigm from feature reuse to dynamic estimation, effectively mitigating cache–input mismatch and preserving generation fidelity.

Acknowledgements

This work was supported by the National Key Research and Development Program of China (No.2023YFC3502900), the National Natural Science Foundation of China (Nos.62176093, 61673182 and 62576139), and the Guangdong Emergency Management Science and Technology Program (No.2025YJKY001).

References

- [1] Black Forest Labs. Flux. <https://github.com/black-forest-labs/flux>, 2024. 1, 2, 5, 7
- [2] Andreas Blattmann, Tim Dockhorn, Sumith Kulal, Daniel Mendelevitch, Maciej Kilian, Dominik Lorenz, Yam Levi, Zion English, Vikram Voleti, Adam Letts, et al. Stable video diffusion: Scaling latent video diffusion models to large datasets. *arXiv preprint arXiv:2311.15127*, 2023. 3
- [3] Huanqia Cai, Sihan Cao, Ruoyi Du, Peng Gao, Steven Hoi, Shijie Huang, Zhaohui Hou, Dengyang Jiang, Xin Jin, Liangchen Li, et al. Z-image: An efficient image generation foundation model with single-stream diffusion transformer. *arXiv preprint arXiv:2511.22699*, 2025. 2
- [4] Junsong Chen, Jincheng Yu, Chongjian Ge, Lewei Yao, Enze Xie, Yue Wu, Zhongdao Wang, James Kwok, Ping Luo, Huchuan Lu, et al. Pixart- α : Fast training of diffusion transformer for photorealistic text-to-image synthesis. *arXiv preprint arXiv:2310.00426*, 2023. 2
- [5] Junsong Chen, Chongjian Ge, Enze Xie, Yue Wu, Lewei Yao, Xiaozhe Ren, Zhongdao Wang, Ping Luo, Huchuan Lu, and Zhenguo Li. Pixart- σ : Weak-to-strong training of diffusion transformer for 4k text-to-image generation. In *European Conference on Computer Vision*, pages 74–91. Springer, 2024. 2
- [6] Pengtao Chen, Mingzhu Shen, Peng Ye, Jianjian Cao, Chongjun Tu, Christos-Savvas Bouganis, Yiren Zhao, and Tao Chen. δ -dit: A training-free acceleration method tailored for diffusion transformers. *arXiv preprint arXiv:2406.01125*, 2024. 1, 3, 5
- [7] Huanpeng Chu, Wei Wu, Guanyu Feng, and Yutao Zhang. Omnicache: A trajectory-oriented global perspective on training-free cache reuse for diffusion transformer models. In *Proceedings of the IEEE/CVF International Conference on Computer Vision*, pages 16302–16312, 2025. 1, 3
- [8] Patrick Esser, Sumith Kulal, Andreas Blattmann, Rahim Entezari, Jonas Müller, Harry Saini, Yam Levi, Dominik Lorenz, Axel Sauer, Frederic Boesel, et al. Scaling rectified flow transformers for high-resolution image synthesis. In *Forty-first international conference on machine learning*, 2024. 1, 2, 3
- [9] Shengjie Gong, Haojie Li, Jiapeng Tang, Dongming Hu, Shuangping Huang, Hao Chen, Tianshui Chen, and Zhuoman Liu. Monocular and generalizable gaussian talking head animation. In *Proceedings of the IEEE/CVF Conference on Computer Vision and Pattern Recognition*, pages 5523–5534, 2025. 5
- [10] Yefei He, Luping Liu, Jing Liu, Weijia Wu, Hong Zhou, and Bohan Zhuang. Ptdq: Accurate post-training quantization for diffusion models. *arXiv preprint arXiv:2305.10657*, 2023. 2
- [11] Jonathan Ho, Ajay Jain, and Pieter Abbeel. Denoising diffusion probabilistic models. *Advances in neural information processing systems*, 33:6840–6851, 2020. 2
- [12] Ziqi Huang, Yinan He, Jiashuo Yu, Fan Zhang, Chenyang Si, Yuming Jiang, Yuanhan Zhang, Tianxing Wu, Qingyang Jin, Nattapol Chanpaisit, et al. Vbench: Comprehensive benchmark suite for video generative models. In *Proceedings of the IEEE/CVF Conference on Computer Vision and Pattern Recognition*, pages 21807–21818, 2024. 6
- [13] Team Hunyuan3D, Shuhui Yang, Mingxin Yang, Yifei Feng, Xin Huang, Sheng Zhang, Zebin He, Di Luo, Haolin Liu, Yunfei Zhao, et al. Hunyuan3d 2.1: From images to high-fidelity 3d assets with production-ready pbr material. *arXiv preprint arXiv:2506.15442*, 2025. 1, 2
- [14] Yang Jin, Zhicheng Sun, Ningyuan Li, Kun Xu, Hao Jiang, Nan Zhuang, Quzhe Huang, Yang Song, Yadong Mu, and Zhouchen Lin. Pyramidal flow matching for efficient video generative modeling. *arXiv preprint arXiv:2410.05954*, 2024. 1, 2
- [15] Kumara Kahatapitiya, Haozhe Liu, Sen He, Ding Liu, Menglin Jia, Chenyang Zhang, Michael S Ryoo, and Tian Xie. Adaptive caching for faster video generation with diffusion transformers. In *Proceedings of the IEEE/CVF International Conference on Computer Vision*, pages 15240–15252, 2025. 1, 3
- [16] Weijie Kong, Qi Tian, Zijian Zhang, Rox Min, Zuozhuo Dai, Jin Zhou, Jiangfeng Xiong, Xin Li, Bo Wu, Jianwei Zhang, et al. Hunyuanvideo: A systematic framework for large video generative models. *arXiv preprint arXiv:2412.03603*, 2024. 1, 2
- [17] Senmao Li, Taihang Hu, Fahad Shahbaz Khan, Linxuan Li, Shiqi Yang, Yaxing Wang, Ming-Ming Cheng, and Jian Yang. Faster diffusion: Rethinking the role of unet encoder in diffusion models. *CoRR*, 2023. 1, 3
- [18] Weiyu Li, Jiarui Liu, Hongyu Yan, Rui Chen, Yixun Liang, Xuelin Chen, Ping Tan, and Xiaoxiao Long. Craftsman3d: High-fidelity mesh generation with 3d native diffusion and interactive geometry refiner. In *Proceedings of the Computer Vision and Pattern Recognition Conference*, pages 5307–5317, 2025. 1, 2
- [19] Weiyu Li, Xuanyang Zhang, Zheng Sun, Di Qi, Hao Li, Wei Cheng, Weiwei Cai, Shihao Wu, Jiarui Liu, Zihao Wang, et al. Step1x-3d: Towards high-fidelity and controllable generation of textured 3d assets. *arXiv preprint arXiv:2505.07747*, 2025. 1, 2
- [20] Yanyu Li, Huan Wang, Qing Jin, Ju Hu, Pavlo Chemerys, Yun Fu, Yanzhi Wang, Sergey Tulyakov, and Jian Ren. Snapfusion: Text-to-image diffusion model on mobile devices within two seconds. *Advances in Neural Information Processing Systems*, 36:20662–20678, 2023. 2
- [21] Yanjing Li, Sheng Xu, Xianbin Cao, Xiao Sun, and Baochang Zhang. Q-dm: An efficient low-bit quantized diffusion model. *Advances in neural information processing systems*, 36:76680–76691, 2023. 2

- [22] Yangguang Li, Zi-Xin Zou, Zexiang Liu, Dehu Wang, Yuan Liang, Zhipeng Yu, Xingchao Liu, Yuan-Chen Guo, Ding Liang, Wanli Ouyang, et al. Triposg: High-fidelity 3d shape synthesis using large-scale rectified flow models. *arXiv preprint arXiv:2502.06608*, 2025. 1, 2
- [23] Zhimin Li, Jianwei Zhang, Qin Lin, Jiangfeng Xiong, Yanxin Long, Xinchu Deng, Yingfang Zhang, Xingchao Liu, Minbin Huang, Zedong Xiao, et al. Hunyuan-dit: A powerful multi-resolution diffusion transformer with fine-grained chinese understanding. *arXiv preprint arXiv:2405.08748*, 2024. 2
- [24] Tsung-Yi Lin, Michael Maire, Serge Belongie, James Hays, Pietro Perona, Deva Ramanan, Piotr Dollár, and C Lawrence Zitnick. Microsoft coco: Common objects in context. In *European conference on computer vision*, pages 740–755. Springer, 2014. 6
- [25] Yaron Lipman, Ricky TQ Chen, Heli Ben-Hamu, Maximilian Nickel, and Matt Le. Flow matching for generative modeling. *arXiv preprint arXiv:2210.02747*, 2022. 2, 3
- [26] Feng Liu, Shiwei Zhang, Xiaofeng Wang, Yujie Wei, Haonan Qiu, Yuzhong Zhao, Yingya Zhang, Qixiang Ye, and Fang Wan. Timestep embedding tells: It’s time to cache for video diffusion model. In *Proceedings of the Computer Vision and Pattern Recognition Conference*, pages 7353–7363, 2025. 1, 3, 5, 7
- [27] Haozhe Liu, Wentian Zhang, Jinheng Xie, Francesco Faccio, Mengmeng Xu, Tao Xiang, Mike Zheng Shou, Juan-Manuel Perez-Rua, and Jürgen Schmidhuber. Faster diffusion via temporal attention decomposition. *arXiv preprint arXiv:2404.02747*, 2024. 1, 3, 5
- [28] Xingchao Liu, Xiwen Zhang, Jianzhu Ma, Jian Peng, et al. InstafLOW: One step is enough for high-quality diffusion-based text-to-image generation. In *The Twelfth International Conference on Learning Representations*, 2023. 2
- [29] Simian Luo, Yiqin Tan, Longbo Huang, Jian Li, and Hang Zhao. Latent consistency models: Synthesizing high-resolution images with few-step inference. *arXiv preprint arXiv:2310.04378*, 2023. 2
- [30] Xinyin Ma, Gongfan Fang, and Xinchao Wang. Deepcache: Accelerating diffusion models for free. In *Proceedings of the IEEE/CVF conference on computer vision and pattern recognition*, pages 15762–15772, 2024. 1, 3
- [31] Chenlin Meng, Robin Rombach, Ruiqi Gao, Diederik Kingma, Stefano Ermon, Jonathan Ho, and Tim Salimans. On distillation of guided diffusion models. In *Proceedings of the IEEE/CVF conference on computer vision and pattern recognition*, pages 14297–14306, 2023. 2
- [32] Alex Nichol, Prafulla Dhariwal, Aditya Ramesh, Pranav Shyam, Pamela Mishkin, Bob McGrew, Ilya Sutskever, and Mark Chen. Glide: Towards photorealistic image generation and editing with text-guided diffusion models. *arXiv preprint arXiv:2112.10741*, 2021. 2
- [33] William Peebles and Saining Xie. Scalable diffusion models with transformers. In *Proceedings of the IEEE/CVF international conference on computer vision*, pages 4195–4205, 2023. 2
- [34] Alec Radford, Jong Wook Kim, Chris Hallacy, Aditya Ramesh, Gabriel Goh, Sandhini Agarwal, Girish Sastry, Amanda Aspell, Pamela Mishkin, Jack Clark, et al. Learning transferable visual models from natural language supervision. In *International conference on machine learning*, pages 8748–8763. Pmlr, 2021. 6
- [35] Aditya Ramesh, Prafulla Dhariwal, Alex Nichol, Casey Chu, and Mark Chen. Hierarchical text-conditional image generation with clip latents. *arXiv preprint arXiv:2204.06125*, 1 (2):3, 2022. 3
- [36] Robin Rombach, Andreas Blattmann, Dominik Lorenz, Patrick Esser, and Björn Ommer. High-resolution image synthesis with latent diffusion models. In *Proceedings of the IEEE/CVF conference on computer vision and pattern recognition*, pages 10684–10695, 2022. 2
- [37] Chitwan Saharia, William Chan, Saurabh Saxena, Lala Li, Jay Whang, Emily L Denton, Kamyar Ghasemipour, Raphael Gontijo Lopes, Burcu Karagol Ayan, Tim Salimans, et al. Photorealistic text-to-image diffusion models with deep language understanding. *Advances in neural information processing systems*, 35:36479–36494, 2022. 2, 3
- [38] Tim Salimans and Jonathan Ho. Progressive distillation for fast sampling of diffusion models. *arXiv preprint arXiv:2202.00512*, 2022. 2
- [39] Axel Sauer, Dominik Lorenz, Andreas Blattmann, and Robin Rombach. Adversarial diffusion distillation. In *European Conference on Computer Vision*, pages 87–103. Springer, 2024. 2
- [40] Pratheba Selvaraju, Tianyu Ding, Tianyi Chen, Ilya Zharkov, and Luming Liang. ForA: Fast-forward caching in diffusion transformer acceleration. *arXiv preprint arXiv:2407.01425*, 2024. 3
- [41] Yuzhang Shang, Zhihang Yuan, Bin Xie, Bingzhe Wu, and Yan Yan. Post-training quantization on diffusion models. In *Proceedings of the IEEE/CVF conference on computer vision and pattern recognition*, pages 1972–1981, 2023. 2
- [42] Junhyuk So, Jungwon Lee, Daehyun Ahn, Hyungjun Kim, and Eunhyeok Park. Temporal dynamic quantization for diffusion models. *Advances in neural information processing systems*, 36:48686–48698, 2023. 2
- [43] Jiaming Song, Chenlin Meng, and Stefano Ermon. Denoising diffusion implicit models. *arXiv preprint arXiv:2010.02502*, 2020. 2
- [44] Yang Song and Prafulla Dhariwal. Improved techniques for training consistency models. *arXiv preprint arXiv:2310.14189*, 2023. 2
- [45] Yang Song, Prafulla Dhariwal, Mark Chen, and Ilya Sutskever. Consistency models. 2023. 2
- [46] Team Wan, Ang Wang, Baole Ai, Bin Wen, Chaojie Mao, Chen-Wei Xie, Di Chen, Feiwu Yu, Haiming Zhao, Jianxiao Yang, et al. Wan: Open and advanced large-scale video generative models. *arXiv preprint arXiv:2503.20314*, 2025. 1, 2, 5, 7
- [47] Xiang Wang, Shiwei Zhang, Han Zhang, Yu Liu, Yingya Zhang, Changxin Gao, and Nong Sang. Videolem: Video latent consistency model. *arXiv preprint arXiv:2312.09109*, 2023. 2
- [48] Chenfei Wu, Jiahao Li, Jingren Zhou, Junyang Lin, Kaiyuan Gao, Kun Yan, Sheng-ming Yin, Shuai Bai, Xiao Xu, Yilei

- Chen, et al. Qwen-image technical report. *arXiv preprint arXiv:2508.02324*, 2025. [1](#), [2](#), [5](#), [7](#)
- [49] Jianfeng Xiang, Zelong Lv, Sicheng Xu, Yu Deng, Ruicheng Wang, Bowen Zhang, Dong Chen, Xin Tong, and Jiaolong Yang. Structured 3d latents for scalable and versatile 3d generation. In *Proceedings of the Computer Vision and Pattern Recognition Conference*, pages 21469–21480, 2025. [1](#), [2](#)
- [50] Jiazheng Xu, Xiao Liu, Yuchen Wu, Yuxuan Tong, Qinkai Li, Ming Ding, Jie Tang, and Yuxiao Dong. Imagereward: Learning and evaluating human preferences for text-to-image generation. *Advances in Neural Information Processing Systems*, 36:15903–15935, 2023. [5](#)
- [51] Chongjie Ye, Yushuang Wu, Ziteng Lu, Jiahao Chang, Xiaoyang Guo, Jiaqing Zhou, Hao Zhao, and Xiaoguang Han. Hi3dgen: High-fidelity 3d geometry generation from images via normal bridging. *arXiv preprint arXiv:2503.22236*, 3:2, 2025. [2](#)
- [52] Richard Zhang, Phillip Isola, Alexei A Efros, Eli Shechtman, and Oliver Wang. The unreasonable effectiveness of deep features as a perceptual metric. In *Proceedings of the IEEE conference on computer vision and pattern recognition*, pages 586–595, 2018. [5](#)
- [53] Xuanlei Zhao, Xiaolong Jin, Kai Wang, and Yang You. Real-time video generation with pyramid attention broadcast. *arXiv preprint arXiv:2408.12588*, 2024. [1](#), [3](#), [5](#), [7](#)
- [54] Yang Zhao, Yanwu Xu, Zhisheng Xiao, and Tingbo Hou. Mobilediffusion: Subsecond text-to-image generation on mobile devices. *arXiv preprint arXiv:2311.16567*, 2(3):4, 2023. [2](#)
- [55] Zangwei Zheng, Xiangyu Peng, Tianji Yang, Chenhui Shen, Shenggui Li, Hongxin Liu, Yukun Zhou, Tianyi Li, and Yang You. Open-sora: Democratizing efficient video production for all. *arXiv preprint arXiv:2412.20404*, 2024. [2](#)
- [56] Xin Zhou, Dingkang Liang, Kaijin Chen, Tianrui Feng, Xiwu Chen, Hongkai Lin, Yikang Ding, Feiyang Tan, Hengshuang Zhao, and Xiang Bai. Less is enough: Training-free video diffusion acceleration via runtime-adaptive caching. *arXiv preprint arXiv:2507.02860*, 2025. [1](#), [3](#), [5](#), [7](#)